Nuclear Instruments and Methods in Physics Research A 602 (2009) 545–551

Contents lists available at ScienceDirect

Nuclear Instruments and Methods in Physics Research A

journal homepage: www.elsevier.com/locate/nima

# Light scattering from an assembly of tracks in a PADC film

D. Nikezic, K.N. Yu *

*Department of Physics and Materials Science, City University of Hong Kong, Tat Chee Avenue, Kowloon Tong, Kowloon, Hong Kong*

ARTICLE INFO

*Article history:*
Received 8 October 2008
Received in revised form
28 January 2009
Accepted 31 January 2009
Available online 12 February 2009

*Keywords:*
PADC
Tracks
Etching
Light
Simulation
Ray tracing

ABSTRACT

A computer program was developed to calculate the light scattered from an assembly of alpha particle tracks in a PADC film. The tracks were randomly seeded on the film to simulate the irradiation by alpha particles emitted by the naturally occurring radon gas and its short-lived progeny. The ray-tracing method was applied to simulate light propagation through the tracks. The angular distribution of scattered light showed a strong maximum between 10° and 20°. The distribution of the scattered light was found to be independent of the equilibrium factor between radon and its progeny. The total amount of scattering increased linearly with the track density and quadratically with the removed layer during chemical etching of the irradiated PADC film.



## 1. Introduction

Solid-state nuclear track detectors (SSNTDs) are commonly used for radon measurements. A recent review on SSNTDs can be found in Ref. [1]. Although counting of tracks in SSNTDs are necessarily related to the light illumination of the detectors, there have been relatively few detailed investigations on the light transmission through the tracks. Groetz et al. [2,3] developed a model based on wave optics for laser light scattering by tracks in polyallyldiglycol carbonate (PADC) films and applied it for neutron dosimetry. Other authors also used scattered light to measure track densities from tracks for neutron dosimetry [4–6]. Recently a model based on geometrical optics to simulate light propagation through the tracks, and to calculate brightness levels of track elements and the track itself was developed [7,8]. The corresponding computer programs were published [9] and are available at http://www.cityu.edu.hk/ap/nru/vision.htm. The model was further expanded to enable determination of the light scattering from a single track [10]. In the present paper, the model was used to calculate light scattering from an assembly of alpha particles tracks in a PADC film, produced by radon and its short-lived progeny.

## 2. Methodology

### 2.1. Geometric model

The model applied here is the same as that described recently for a single track [9,10], so it will not be elaborated again in detail. However, when light is scattered by a track assembly created by randomly incident alpha particles, there are some differences when compared to the case for a single track, which will be addressed here.

When a single track was considered, the $z$-axis was normal to the detector surface, the $x$-axis was on the post-etching surface of the detector and was along the major axis of the track, and the $y$-axis was normal to the $x$-axis and was also on the post-etching surface of the detector. However, in the case of irradiation by radon and its progeny, there will be tracks with all possible orientations with respect to the angle $\varphi$ as shown in Fig. 1, in which two tracks $T_1$ and $T_2$ are presented. The major axis of the track $T_1$ overlaps with the $x$-axis of the coordinate system, and the track center coincides with the origin of the coordinate system. In our previous work, the light scattering was calculated only from tracks located at $T_1$.

Track $T_2$ is located at another position in the detector, and it is analyzed in the following ways: (1) the origin of the coordinate system was translated to the center of $T_2$ and the system was then rotated for the angle $\varphi$; (2) the scattering of light was then calculated from $T_2$ in the new translated and rotated coordinate system; (3) the last step was to return back to the basic coordinate system $xOy$. The calculated scattering pattern from a single track had to be rotated back for the angle $-\varphi$.

In our model, a circular PADC film with an area of 1 cm$^2$ was considered, and the origin of the coordinate system was chosen to be at the center of the detector. Although it would be difficult in reality to cut a piece of PADC film in a circular shape, this geometry was adopted for the sake of simplicity. To calculate the intensity of the scattered light, a hemisphere with a radius of 10 cm (ensuring that it was much larger than the radius of

* Corresponding author. Tel.: +852 27887812; fax: +852 27887830.
*E-mail address:* peter.yu@cityu.edu.hk (K.N. Yu).

0168-9002/$ - see front matter © 2009 Elsevier B.V. All rights reserved.
doi:10.1016/j.nima.2009.01.204

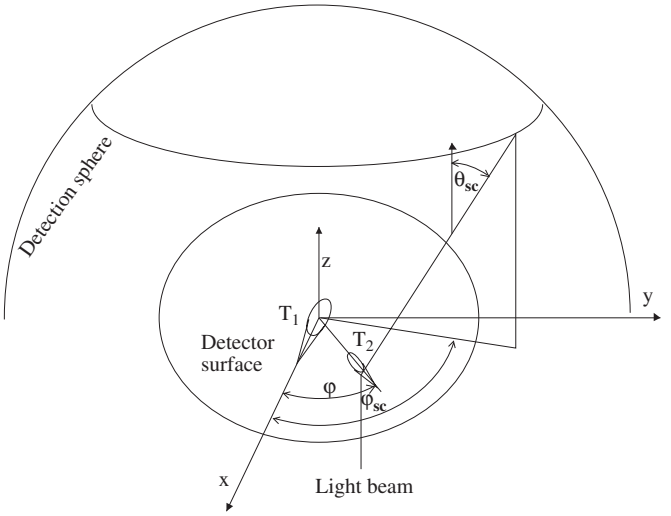


**Fig. 1.** Coordinate system employed for the present study. The major axis of the track $T_1$ lies along the $x$-axis. The tip of $T_1$ is in the $xOz$ plane. The major axis of the track $T_2$ is determined with the angle $\varphi$. The detection hemisphere is also shown.

detector) was constructed with its center located at the origin. A scattered light ray that exited from the detector material should intersect with the hemisphere at a point that could be determined by the angles $\varphi_{sc}$ and $\theta_{sc}$, and these angles determined the approximate scattering direction. The situation is also illustrated in Fig. 1, where one light beam is scattered by $T_2$.

### 2.2. Sampling of alpha particles and seeding tracks in the PADC film

It was assumed that the tracks in the PADC film originated from alpha particles emitted by radon ($^{222}$Rn) and its short-lived progeny $^{214}$Po and $^{218}$Po, with energies 5.49, 6 and 7.69 MeV, respectively. A mixture of radon and its progeny in air is usually characterized by the so-called "equilibrium factor" (see, e.g., Refs. [11–13] and references therein). The Monte Carlo simulation started with the sampling of an emitter which could be $^{222}$Rn, $^{214}$Po or $^{218}$Po. If the concentrations of these alpha particle emitters are denoted as $C_0$, $C_1$ and $C_4$, respectively, the total alpha particle activity $C_{tot}$ is given by $C_{tot}=(C_0+C_1+C_4)$. Three ratios were defined as $A=C_0/C_{tot}$, $B=C_1/C_{tot}$ and $C=C_4/C_{tot}$. The standard method of discrete event sampling was applied to "choose" an alpha particle as follows. The random number generator was invoked to get one random number $\gamma$; if $\gamma<A$, the emitter was chosen as $^{222}$Rn; if $A<\gamma<(A+B)$, the emitter was $^{218}$Po; and if $(A+B)<\gamma<1$, the emitter was $^{214}$Po. After choosing the emitter (and thus the corresponding alpha particle energy), the emission point and direction were also sampled.

The next step in the simulation was to check whether the alpha particle hit the detector considering its flight direction and range in air. If not, this alpha particle was discarded and the simulation loop was restarted, choosing a new alpha particle. Obviously, the cases where the alpha particles hit the detector and left latent tracks in it were more important. If a visible track was formed from that latent track due to subsequent chemical etching, the three-dimensional coordinates of the track were calculated. The last step involved the simulation of light propagation through the track and calculations of the angular distribution (in $\varphi$ and $\theta$) of the scattered light. To perform the last step of simulation, a computer program TRACK_VISION.F90 described previously in Ref. [9] was used as a subroutine. Information about the scattering direction was stored in the computer memory. After this, the construction of one track was completed. A new alpha particle was then chosen and all the procedures were repeated again. The intensity of light scattered from a track in a particular direction was added to the total intensity in that direction summed from previous calculations, so that the result for a given assembly of tracks could be obtained. The simulation was terminated when the predetermined number of tracks was achieved.

One specific problem is noted here. The tracks obtained as mentioned above could be very different in size and shape with various scattering characteristics. Here, a track was represented as a mesh of planar elements with a size of approximately of $1\times1\,\mu m^2$. Our model did not represent a track with elements having exactly the same surface area. Each element scattered light in a defined direction. The intensity of light scattered by some element had then to be multiplied with a weighting factor $\omega_i$, which was equal to the ratio between the surface area of the $i$th element (projected onto the detector surface) and the total surface area of the detector.

### 2.3. Conditions for calculations

The following were employed in the calculations:

- Bulk etch rate $V_b=1.2\,\mu m/h$. This value was based on our previous measurements and corresponded to the following etching conditions: 6.25 N aqueous solution of NaOH at 70 °C [14].
- $V$ function for alpha particle tracks in a PADC film from [15–18].
- Refractive index of 1.5 for a PADC film [16].

## 3. Results

### 3.1. Changes in opening surface area with etching time

A parameter that significantly affects the amount of scattered light is the projected surface area of the track. The calculated track parameters are dependent on the $V$ function being used in the calculations. In order to examine the effects of using different $V$ functions on the track surface area, calculations were performed for three $V$ functions found in the literature [15–17]. Calculations were performed for normal incidence and for incident energies of 1, 3, 5 and 7 MeV. The results are shown in Fig. 2.

As expected, the surface area of the track opening increases with the etching time. Differences arising from using different $V$ functions are readily noticeable. The track opening areas calculated using the $V$ function from Ref. [15] were above those calculated using the other two $V$ functions for incident energies of 1, 3 and 5 MeV. For the incident energy of 7 MeV, the results calculated using the $V$ function from Ref. [15] became smaller than those from Ref. [16]. The results calculated using the $V$ function from Ref. [17] are consistently the lowest. Other research groups also made comparisons among the various $V$ functions found in the literature and also compared them using experimental data [19,20]. Rana [19] showed that the experimental data for track openings were between the predictions obtained with $V$ functions from Refs. [15,16] and the $V$ function from Ref. [17]. On the other hand, Hersmdorf and Hunger [20] found that $V$ functions from Refs. [15] and [17] had the largest and smallest values, respectively, while that from Ref. [16] was in between. The findings in Refs. [19] and [20] are consistent with those shown in Fig. 2. Hersmdorf and Hunger [20] also found a new parametric function which agreed well with their experimental data and with the function given in Ref. [15]. However, the experimental data on

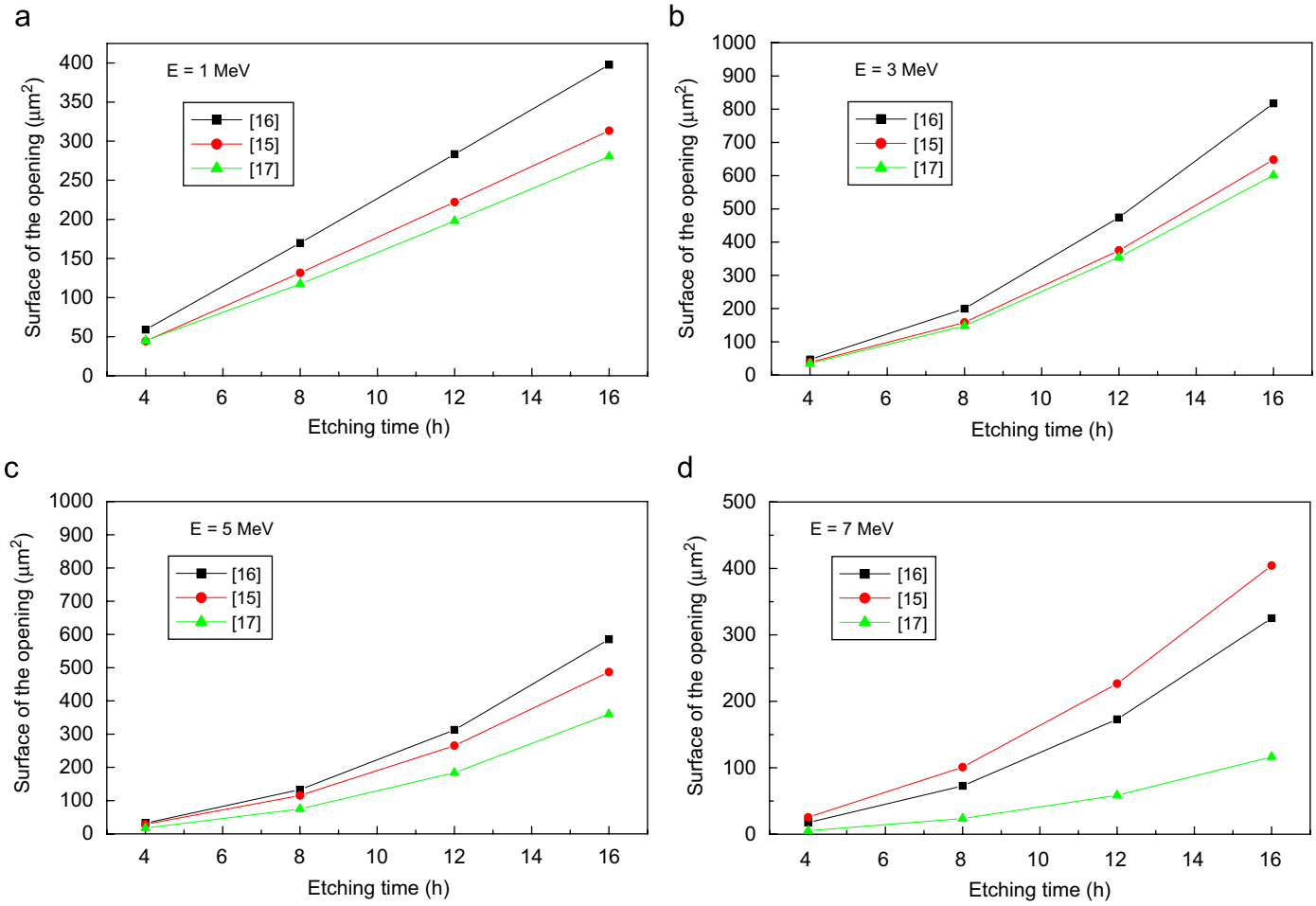


**Fig. 2.** Surface area of track opening as a function of etching time calculated using three different $V$ functions, for incident energies: (a) 1 MeV; (b) 3 MeV; (c) 5 MeV; (d) 7 MeV.

track parameters were not yet in full agreement with the published $V$ functions. This strongly called for continued work on attempts to obtain more accurate $V$ functions for the PADC detector.

The distribution of scattered light with respect to the angle $\varphi$ was found to be uniform. This result was expected because the tracks in all directions with respect to the angle $\varphi$ could be found in a detector irradiated by radon and its progeny. The data for the distribution in the angle $\varphi$ will not be presented here; only the distributions with respect to the angle $\theta$ will be presented.

### 3.2. Distribution of scattered light with equilibrium factor as a parameter

Three groups of calculations were performed. The first one was related to variations in the progeny ratios, which would lead to variations in the equilibrium factor. The parameters $F_i$ used in Fig. 3 is the ratio of the concentration $C_i$ of the $i$th radon progeny ($i = 1$ or 4) to the radon gas concentration $C_0$, i.e., $F_i = C_i/C_0$. The data are presented in Fig. 3(a)–(c) for different etching time of 4, 8 and 14 h (corresponding to removed layers of 4.8, 9.6 and 16.8 μm according to the bulk etch rate measured in Ref. [14]), respectively. The initial light intensity is denoted as $I_0$. The light that was transmitted through the undamaged part of the detector was not scattered (for $\theta = 0^\circ$). Since the majority of the detector was not damaged, the intensity of the non-scattered light should be much larger than that of the scattered light, and the former is not shown in the figures.

From Fig. 3, we can see that the distributions have maximums between 10° and 20° and fall to very small values beyond 50°. The scattered intensity weakly depends on the assumed ratios between the concentrations of the alpha particle emitters. In fact, the differences among the curves corresponding to various equilibrium factors probably originated from statistical errors in the calculations. As such, it will be very difficult to develop a method to determine the equilibrium factor based on the angular distribution of scattered light.

In addition to scattering at small angles, the light could be scattered at very large angles, up to 80°, but with very small intensities. These results are better seen in semi-logarithmic presentations shown as insets in Fig. 3(a)–(c).

In Fig. 3(c), the relationship for the scattered light intensity is presented for the same equilibrium factors as those shown in Fig. 3(a) and (b), but for an etching time of 14 h (corresponding to 16.8 μm of removed layer during chemical etching). The dependence on the radon progeny ratios is still very weak (viz., all curves are close to each other). In this case, there is also scattering for angles larger than 50° as illustrated in the semi-logarithmic presentation. Here, for large scattering angles, distinction among the curves corresponding to different equilibrium factors is again very weak, and it is again dubious whether this small separation can be used for determination of the equilibrium factor, considering the very low intensity of light scattered at large angles.

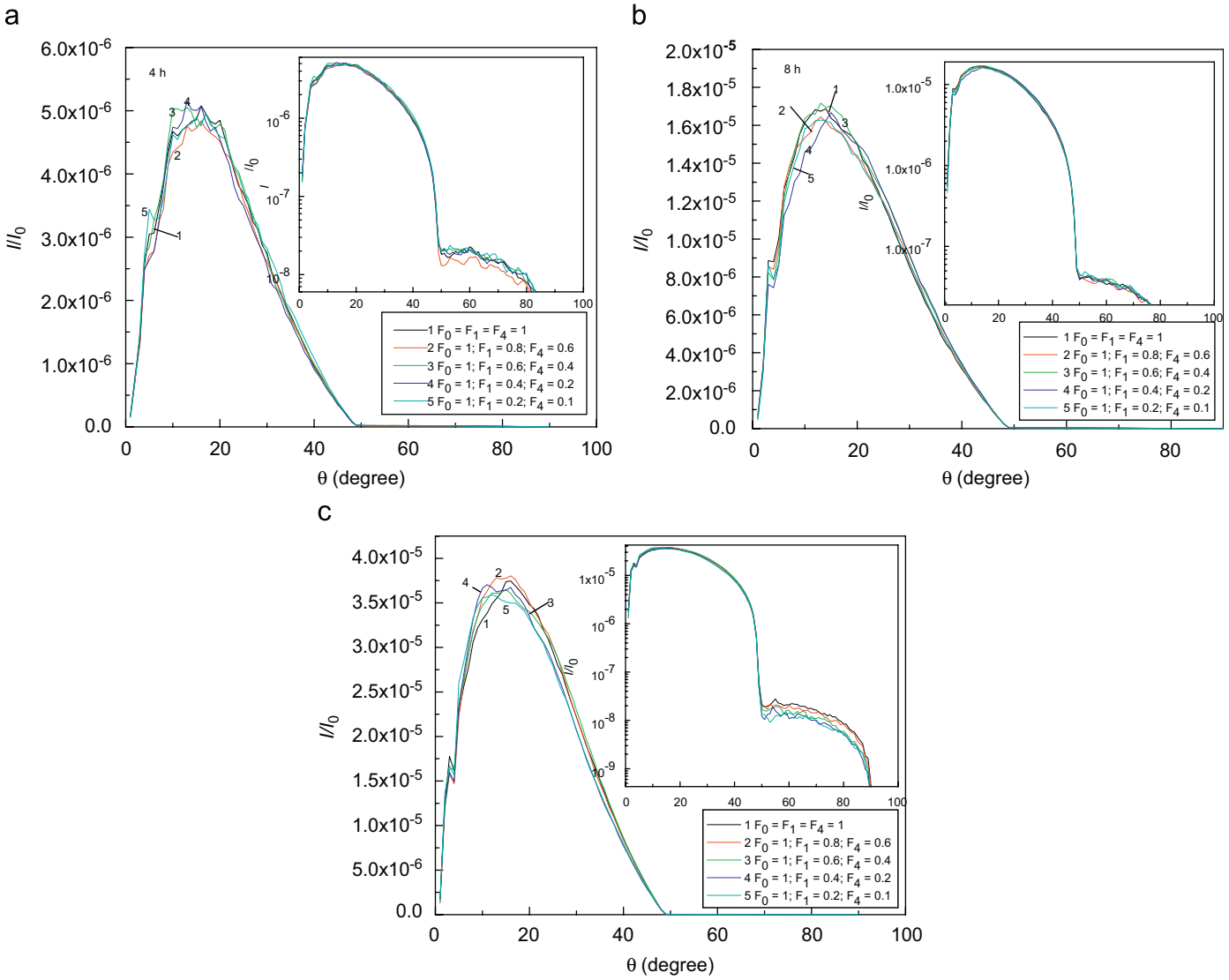


**Fig. 3.** Distribution of scattered light intensity with respect to the angle $\theta$ for different ratios of $F_1$ and $F_4$. In the simulations, the whole interval of angle $\theta$ between 0° and 90° was divided in 90 intervals, with increments of 1°. Calculations have been performed for 1000 tracks on a 1 cm$^2$ PADC film: (a) for 4 h of etching (4.8 μm of removed layer); (b) for 8 h of etching; (c) for 14 h of etching. Insets show the semi-logarithmic presentations.

The shape of the distributions shown in Fig. 3(a)–(c) is practically the same and does not depend on the chemical etching time; the maximums are approximately at the same position between 10° and 20°. However, comparison among Fig. 3(a)–(c) shows that the absolute values of the scattered light intensity are the largest for 14 h of etching. This is in fact expected since larger-size tracks obtained for longer etching will engage more light for scattering.

A qualitative explanation for the existence of large and small scattering angles is given in Fig. 4.

Two typical tracks are presented in Fig. 4. The left one is in the sharp conical phase and can scatter light only through large angles. The light beam comes from the bottom (considering the transmission mode operation of the microscope here) and undergoes total reflection on the track wall. The beam then comes to the post-etching detector surface where it is refracted and scattered under a very large angle. Total reflection is also possible at the detector surface (not shown in Fig. 4), after which the light beam comes back into the detector body. This track will appear completely dark under the optical microscope, since the objective lens will not collect the light rays scattered from this track through very large angles.

Two different cases are shown on the right-hand side of Fig. 4, where a track in the spherical phase is presented. Light beam 1 will be scattered through small angles. Scattering through large angles from spherical tracks is also possible; an example is shown as light beam 2 on the right-hand side of Fig. 4. If the etching time is shorter, more tracks are in the sharp conical phase, so more scattering through large angles can be expected. We can compare the maximal value of scattering intensity (i.e., at the peak), and the scattering intensity at a chosen angle, say 60°. The comparisons are shown in Table 1. The average values for five curves shown in Fig. 3(a)–(c) are calculated and presented in Table 1.

A simple inspection of the numbers in Table 1 reveals that an increase in the removed layer during etching will cause

(1) a significant increase in the intensity of the scattered light at the peak region (angle = 15°) (~7.5 times from 4 to 14 h of etching);

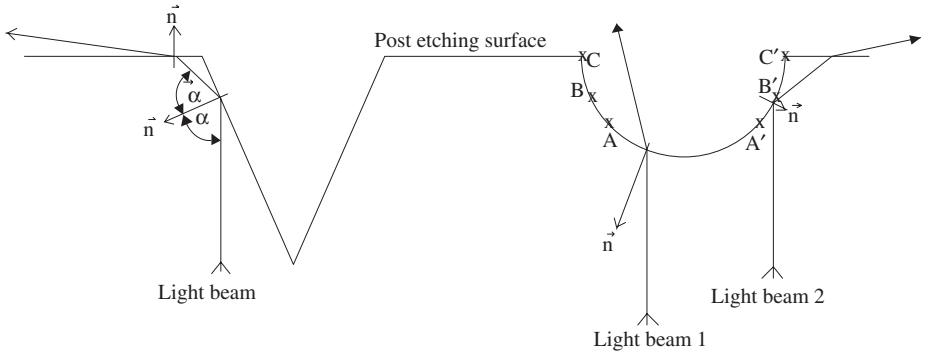


**Fig. 4.** Scattering of light for a track in the sharp conical phase (*left*) and a track in the spherical phase (*right*). Two different cases are shown for the spherical track. $\vec{n}$ is normal to the surface at the point where the light beam is reflected or refracted. The transmission mode of the optical microscope is considered.

**Table 1**
Ratios of the scattered light intensity $I$ to the initial intensity $I_o$ at the peak (angle = 15°) and at the tail (angle = 60°), and their ratios.

| Etching time (h) | $I/I_0$ (15°) | $I/I_0$ (60°) | $[I/I_0\ (15°)]/[I/I_0\ (60°)]$ |
|---|---|---|---|
| 4 | $4.843 \times 10^{-6}$ | $2.053 \times 10^{-8}$ | 242 |
| 8 | $1.640 \times 10^{-5}$ | $3.797 \times 10^{-8}$ | 432 |
| 14 | $3.664 \times 10^{-5}$ | $1.657 \times 10^{-8}$ | 1907 |

(2) not too much change, or even a decrease, in the intensity of scattered light at large angles;
(3) a significant increase in the ratio of scattered intensities at 15° and 60°, which is a consequence of the outcomes in items (1) and (2) above.

The intensity of light scattered from a surface element of a track is proportional to its projected area on the post-etching detector surface. In other words, the inclination of the element and its surface area are defining the amount of light incident on that surface and scattered from it (or reflected if total reflection takes place). For example, on the right-hand side of Fig. 4, the light beams incident on the track surface between points $A$ and $A'$ will be refracted through small angles; those between $A$ and $B$ will be scattered through large angles; and those between $B$ and $C$ will again contribute to scattering through small angles or to total reflection. Projected areas on the post-etching surface of elements which scatter light through small angles are in general much larger than those through large scattering angles. In the case of prolonged chemical etching, more and more tracks will have reached the spherical phase so more light rays will be scattered through small angles. This explains the shape of curves in Fig. 3 and the data in Table 1. This simplified analysis of two different tracks shown in Fig. 4 is only for illustration purposes. In the case for realistic exposures to radon and its progeny, there are tracks with many different shapes and sizes, which originate from irradiation by alpha particles with all possible incident angles and energies. It is remarked here that an exact analysis or analytical treatment of light scattering from such a variety of tracks would be very difficult.

### 3.3. Effects of V function on distribution of scattered light intensity

As discussed above, the estimated surface area of the track depends on the $V$ function used in the calculations. As a consequence, the distribution and intensity of scattered light are also dependent on the $V$ function. Fig. 5 shows the results obtained under the same conditions except for four different $V$ functions taken from Refs. [15–18], for etching time of 4 h (Fig. 5(a)) and 8 h (Fig. 5(b)). The distributions of scattered light intensity obtained with different $V$ functions have similar shapes

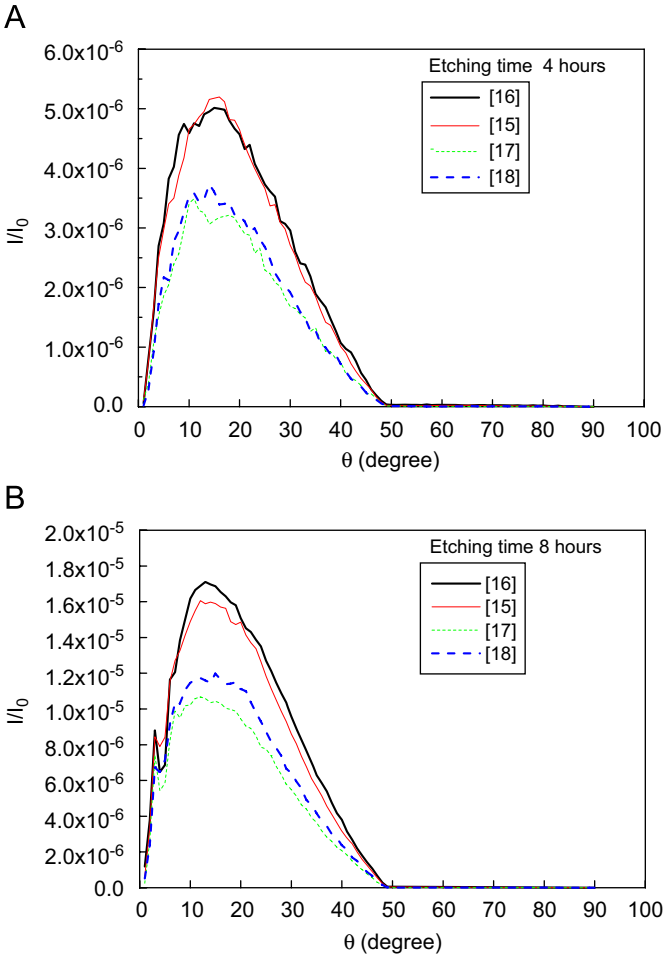


**Fig. 5.** Distribution of scattered light intensity with respect to the angle $\theta$ for four different $V$ functions.

but with different magnitudes: those obtained with functions from Refs. [15] and [16] are close to each other, while those obtained with functions from Refs. [17] and [18] are also close to each other.

### 3.4. Scattered light intensity vs track density

The scattered light intensity is dependent on the track density. This is expected since more tracks will scatter more light. To study this dependence, the number of tracks on a 1 $cm^2$ detector surface was varied between 100 and 2000 for the three different etching times of 4, 8 and 12 h. The results are given in Fig. 6. The ordinate

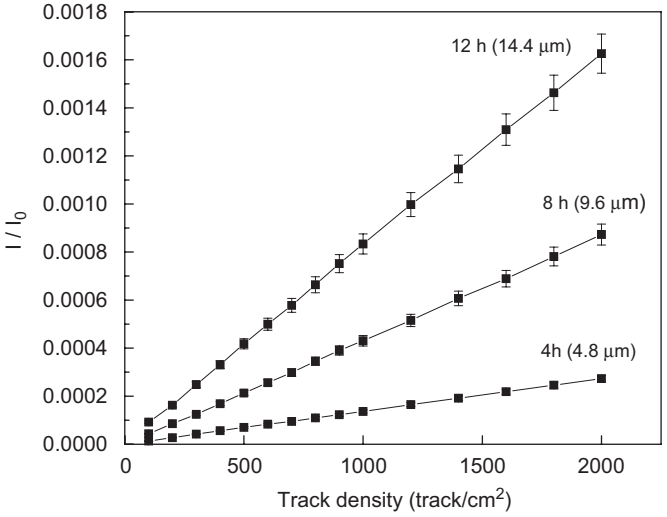


**Fig. 6.** Relative intensity of the scattered light as a function of the track density, with the etching time in h (or removed layer in μm) as a parameter.

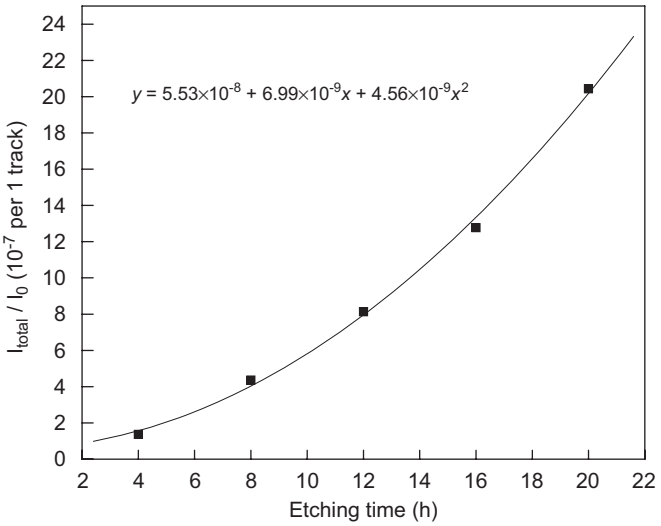


**Fig. 7.** Dependence of the total amount of scattering intensity $I_{total}$ per one track as a function of etching time. The scattered points were obtained by calculations, and the solid line was a quadratic fit. $F_1 = 0.8$, $F_4 = 0.4$ and bulk etch rate $V_b = 1.2$ μm/h [14].

gives the ratio $I/I_0$, where the total scattered light $I$ is evaluated by integrating over all angles $\varphi$ (between 0 and $2\pi$) and $\theta$ (between 0 and $\pi$). A linear dependence is apparent, which is very promising in enabling a practical application. The increase in the scattered intensity with the etching time is expected because larger tracks scatter more light.

### 3.5. Scattered light intensity vs etching time

The dependence of the total amount of scattering $I_{total}$ (evaluated by integrating over all angles $\theta$ and $\varphi$ as described above), given by $I_{total}/I_0$ per one track, on the etching time is presented in Fig. 7, where the following conditions have been considered: $F_1 = 0.8$, $F_4 = 0.4$ and bulk etch rate $V_b = 1.2$ μm/h [14]. The increase seems to be quadratic, with the fitting formula and the best-fit line also shown.

The quadratic increase of $I_{total}$ is reasonable because the surface area of a track increases with the etching time. For example, Fig. 8

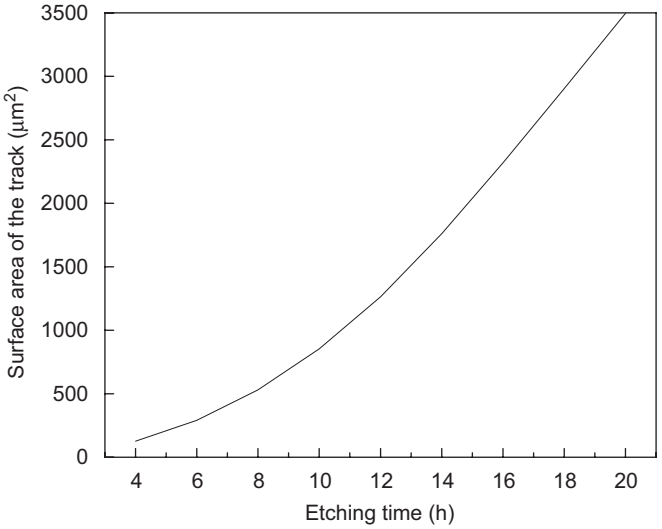


**Fig. 8.** Dependence on the etching time of the area of a track generated by an alpha particle with the incident energy of 3.2 MeV and with normal incidence.

shows the variation of the area of a track generated by an alpha particle with the incident energy of 3.2 MeV and with normal incidence. In the case of irradiation by alpha particles from radon and its progeny, tracks with different incident angles and energies are possible, but the quadratic increase is preserved.

## 4. Discussion

Two very interesting phenomena were observed in the present study. The first one was the independence (or very weak dependence) of the distribution of the scattered light on the equilibrium factor. The second one was the *linear* dependence of the scattered light intensity on the track density. These will be discussed in more detail in the following.

If the equilibrium factor is equal to 1, which is never achieved in reality, equal numbers of alpha particles with energies of 5.49, 6 and 7.69 MeV are expected to be emitted from a unit volume of air per unit time. For a smaller equilibrium factor (which is caused by ventilation and/or plateout), smaller percentages of higher-energy alpha particles (6 and 7.69 MeV) are expected. If the equilibrium factor is very small, alpha particles with 5.49 MeV energy are more frequently emitted than others. To explain the independence of the scattered intensity of the equilibrium factor, we revisit the incident energy spectrums of alpha particles presented in Fig. 9, which is adopted from Ref. [21].

In Fig. 9, the spectrums of alpha particles incident onto the detector surface for two extreme situations are presented, namely for equilibrium factors $F = 1$ and 0.1. If $F = 0$, which is unrealistic, there will be a vertical drop at 5.49 MeV and no alpha particles with larger energies will be emitted. All realistic situations are located between the curves for the two extreme cases. A closer study will reveal that the incident spectrums are different in these two cases, but not significantly. For example, if $F_1 = 1$ and $F_4 = 1$, which is the case for an equilibrium factor $F = 1$, there will be 18.1% of alpha particles with energies between 6 and 7.69 MeV incident onto the detector. If these ratios are reduced to $F_1 = 0.2$ and $F_4 = 0.1$, the fraction of particles between 6 and 7.69 MeV will drop to 4.5%. By increasing the equilibrium factor $F$ from 0.1 to 1, the number of alpha particles with energies between 6 and 7.69 MeV incident on the detector increases by only 14% (i.e., from 4% to 18%).

On the other hand, alpha particles with larger energies will create smaller tracks in the PADC film, and these tracks will also

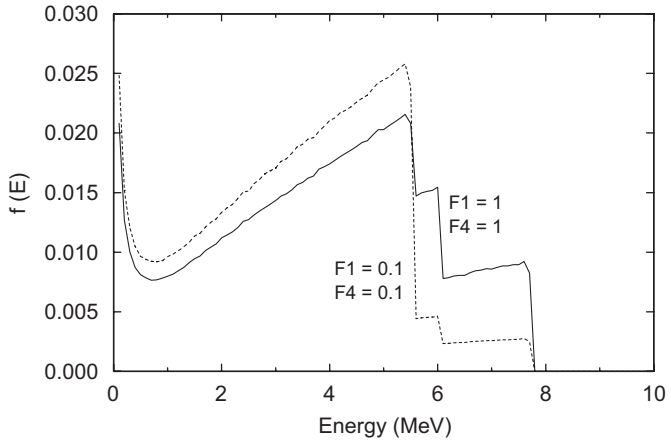


**Fig. 9.** Spectrums of alpha particles from radon and its progeny incident onto the detector surface for two extreme cases ($F = 1$ and 0.1) [17].

be in the sharp conical phase (except for prolonged etching) [22]. As explained above, the total amount of light scattered from a track is proportional to its surface area projected on the post-etching detector surface, noting that the shape of the track and the inclination angle also play important roles. If the etching time is short (e.g., 4 h), the small tracks formed by the high-energy alpha particles would scatter only a relatively small amount of light, which is not enough to create a significant difference that can be used to distinguish between different equilibrium factors. If the etching time is longer (14 h), all tracks will have reached the spherical phase so the shape of tracks will become independent of the initial alpha particle energy. Again, information on the equilibrium factor is lost here.

The second phenomenon, i.e., the *linear* dependence of the scattered light intensity on the track density, is more readily comprehensible. The total amount of light scattered from an assembly of tracks is proportional to their surface area. If the number of tracks is increased, say by $n$ times, the encompassed surface would also be increased by $n$ times, with the tracks randomly seeded on the detector. This explains the linear dependence of the total amount of scattered light on the number of tracks. The limitation here is the possible overlapping of tracks for very large track densities, which, however, can be avoided through careful experimental design and will therefore not be considered in the present work.

## 5. Conclusions

The conclusions reached in the present study are briefly summarized here:

(1) The distribution of the scattered light intensity with respect to the angle $\varphi$ is uniform. This is a consequence of random orientation of tracks in the assembly, which is expected in the case of irradiation by alpha particles from radon and its progeny. This is also a consequence of the symmetry of an alpha particle track with respect to the particle trajectory.
(2) The distribution of the scattered light with respect to the angle $\theta$ has a maximum between 10° and 20°, and drops to very small values beyond about 50°. However, it is possible to find scattered light through very large angles, e.g., about 80°. Scatterings through angles close to 90° are also possible but are very weak. It is interesting to note that this distribution does not depend on the equilibrium factor.
(3) The maximum between 10° and 20° increases significantly with the etching time, and more light is scattered through small angles with prolonged etching.
(4) The total amount of scattered light depends linearly on the track density, and quadratically with the removed layer during chemical etching of the irradiated film.

## Acknowledgement

The present work was supported by a research grant CityU123106 from the Research Grants Council of the HKSAR.

## References

[1] D. Nikezic, K.N. Yu, Mater. Sci. Eng. R 46 (2004) 51.
[2] J.E. Groetz, A. Lacourt, A. Chambaudet, Nucl. Instr. and Meth. B 142 (1998) 503.
[3] J.E. Groetz, A. Lacourt, P. Meyer, M. Fromm, A. Chambaudet, J. Potter, Radiat. Prot. Dosim. 85 (1999) 447.
[4] J.R. Harvey, A.R. Weeks, Radiat. Prot. Dosim. 20 (1987) 89.
[5] P. Meyer, J.E. Groetz, M. Fromm, A. Lacourt, A. Chambaudet, Radiat. Meas. 28 (1997) 423.
[6] P.C. Popov, D.S. Pressyanov, Radiat. Meas. 27 (1997) 27.
[7] D. Nikezic, F.M.F. Ng, C.W.Y. Yip, K.N. Yu, Radiat. Meas. 40 (2005) 375.
[8] K.N. Yu, H.H.W. Lee, A.W.T. Wong, Y.L. Law, S.F.L. Cheung, D. Nikezic, F.M.F. Ng, Nucl. Instr. and Meth. B. 263 (2007) 271.
[9] D. Nikezic, K.N. Yu, Comput. Phys. Commun. 178 (2008) 591.
[10] D. Nikezic, K.N. Yu, Radiat. Meas. 43 (2008) 1417.
[11] D. Nikezic, F.M.F. Ng, K.N. Yu, Appl. Radiat. Isot. 61 (2004) 1431.
[12] K.N. Yu, D. Nikezic, F.M.F. Ng, J.K.C. Leung, Radiat. Meas. 40 (2005) 560.
[13] K.N. Yu, S.Y.Y. Leung, D. Nikezic, J.K.C. Leung, Radiat. Meas. 43 (Suppl. 1) (2008) S357.
[14] J.P.Y. Ho, C.W.Y. Yip, D. Nikezic, K.N. Yu, Radiat. Meas. 36 (2003) 141.
[15] C. Brun, M. Fromm, M. Jouffroy, P. Meyer, J.E. Groetz, F. Abel, A. Chambaudet, B. Dorschel, D. Hermsdorf, R. Bretschneider, K. Kadner, H. Kuhne, Radiat. Meas. 31 (1999) 89.
[16] S.A. Durrani, R.K. Bull, Solid State Nuclear Track Detection: Principles, Methods and Applications, Pergamon Press, Oxford, 1987.
[17] K.N. Yu, F.M.F. Ng, D. Nikezic, Radiat. Meas. 40 (2005) 380.
[18] K.N. Yu, J.P.Y. Ho, D. Nikezic, C.W.Y. Yip, Determination of the $V$ function for CR-39 by atomic force microscope, in: A. Mendez-Vilas (Ed.), Recent Advances in Multidisciplinary Applied Physics, Elsevier, Amsterdam, 2005.
[19] M.A. Rana, Radiat. Meas. 43 (2008) 1546.
[20] D. Hersmdorf, M. Hunger, Evaluation of the sensitivity function $V$ for registration of α-particles in CR-39 SSNTDs. Paper presented at 24th International Conference on Nuclear Tracks in Solids, Bologna, Italy, 1–5 September 2008.
[21] D. Nikezic, K.N. Yu, Nucl. Instr. and Meth. B. 187 (2002) 492.
[22] D. Nikezic, K.N. Yu, Comput. Phys. Commun. 174 (2006) 160.